Non-linear waveform and delay time analysis of triplicated core phases

R. Garcia

Département de Géophysique Spatiale et Planétaire, IPGP, CNRS

UMR7096, 94107 St Maur des Fossés, France.

S. Chevrot

Laboratoire de Dynamique Terrestre et Planétaire, CNRS UMR5562, 31400

Toulouse, France.

M. Weber

GeoForschungsZentrum, Section 2.2 "Deep Seismic Sounding", D-14473

Potsdam, Germany.

R. Garcia, Département de Géophysique Spatiale et Planétaire, IPGP, CNRS UMR7096, 4, Ave de Neptune, 94107 St Maur des Fossés, France. (garcia@ipgp.jussieu.fr)

Abstract. We introduce a new method to measure differential travel times and attenuation of seismic body waves. The problem is formulated as a non linear inverse problem which is solved by simulated annealing. Using this technique, we have analysed triplicated PKP waves recorded by the temporary EIFEL array in central Europe. These examples demonstrate the potential of the technique, which is able to determine differential traveltimes and waveforms of the core phases, even when they interfere on the seismograms or when additional depth phases are present. The PKP differential travel times reveal the presence of large amplitude and small scale heterogeneities along the PKP(AB) ray paths, and favour an inner core model with 0.8% velocity perturbation in its top 150 km and small velocity perturbations below. The estimate of PKP differential attenuation puts a lower bound of 50 on the inner core quality factor in the top 300 km of the inner core.

1. Introduction

The arrival times of body waves are the primary source of information exploited in the seismological records. Large data sets have been created *Engdahl et al.* [1998] which allowed tomographic studies at both regional and global scales *Van der Hilst et al.* [1997]; *Bijwaard et al.* [1998]. The growth of data recorded by seismic networks during the past decade has motivated the search for new methods to measure routinely body wave arrival times. Classically, these methods are based on cross correlations between the different records of a network *VanDecar and Crosson* [1990]. In a previous paper, Chevrot (2002) has described a non linear algorithm that permits the estimation of the optimal waveform recorded by all the stations of a seismological network, and its time delays at each station. While the analysis of seismograms containing a single prominent seismic phase is relatively simple, seismologists often face complex records where different seismic phases interfere. To demonstrate that the same approach can also be used on such records, we have generalized the algorithm to the case of interfering waves. We focus on the analysis of seismograms in the distance range of the PKP triplication. On these kind of records, interference is particularly strong. We invert for the reference PKP(BC) waveform recorded by all the stations, and describe the other body waves as functionals of this reference waveform. This approach therefore incorporates some a priori information in the inversion process.

The paper is organized as follows. Section 2 presents the model parametrization, the a priori information and the simulated annealing algorithm. Section 3 shows examples of applications on triplicated core phases recorded by the EIFEL experiment. These examples are chosen in order to demonstrate the potential of the method. The differential travel

times and attenuations are analysed to extract informations on the Earth core structure in section 4. Finally, we dicuss the advantages and shortcomings of this approach, and present several possible applications.

2. Method

2.1. A priori information and model parameterization

The triplication of PKP, the P-phase propagating inside the core, occurs in the epicentral distance range 146°-153°. Three core phases interfere: PKP(DF) which has its turning point inside the strongly attenuating inner core, PKP(BC) which turns at the base of the liquid core, and PKP(AB) which turns in the middle of the liquid core, and is proportionnal to the Hilbert transform of PKP(BC) *Choy and Richards* [1976]; *Creager* [1992]; *Song* [1997]; *Garcia and Souriau* [2000, 2001]. The ray paths of the three core phases are shown on figure 1. With a good approximation, the seismic records of the PKP triplication can be modelled as a sum of three seismic phases:

$$S_i(t) = R_{DF} A(t_i^*) * W(t + \tau_i^{DF}) + W(t + \tau_i^{BC}) + R_{AB} H * W(t + \tau_i^{AB}) \qquad (1)$$

where $S_i(t)$ is the seismogram recorded by station number i, $W(t)$ is the waveform of the PKP(BC) phase taken as a reference, $A(t_i^*)$ is a differential attenuation operator, H is the Hilbert transform operator, R_{DF} and R_{AB} are real numbers describing amplitude corrections, and τ_i^{DF}, τ_i^{BC} and τ_i^{AB} are the time shifts of the PKP(DF), PKP(BC) and PKP(AB) phases respectively, relative to the beginning of the record. The attenuation operator is defined by $A(t^*) = \exp(-\pi f t^*) \exp\left(2if \ln(\frac{f}{f_0}) t^*\right)$, where f is the frequency, and $f_0 = 2$ Hz is the reference frequency of PKP(DF). This description contains our prior knowledge of the seismic records in the triplication distance range. The model space

is thus described by the time samples of the reference waveform $W(t)$, the amplitude corrections R_{DF} and R_{AB}, and by the different times t_i^*, τ_i^{DF}, τ_i^{BC} and τ_i^{AB} related to each record i.

In the formulation of the problem, we make the implicit assumptions that the source time function is not affected by directivity effects, and that the waveforms are not strongly distorted by mantle heterogeneity. Additionally, we assume that PKP(AB) is the Hilbert transform of the PKP(BC) phase, and that the PKP(DF) phase has the same waveform as the PKP(BC) phase, but attenuated. The PKP(DF) phase passing through the inner core is more attenuated than the PKP(BC) phase which travels only in the outer core where the attenuation is very low *Doornbos* [1983]; *Souriau and Roudil* [1995]; *Cormier et al.* [1998]. Because PKP(BC) and PKP(DF) phases follow approximately the same ray paths in the crust and the mantle, only short wavelength heterogeneities in the D" layer can distort their relative waveforms *Bréger et al.* [1999]. However, PKP(AB) and PKP(BC) phases follow slightly different ray paths in the mantle, resulting in a larger sensitivity to lateral variations in seismic velocities, particularly in the D" layer *Bréger et al.* [2000]; *Tkalčić et al.* [2002]. The network size must not be too large in order to avoid strong waveform variations over the network owing to crustal heterogeneities and directivity effects at the source.

A priori information is also introduced by imposing conditions on the relative time shifts between the different seismic phases. Admissible variations of the differential travel time residuals (BC-DF) and (AB-BC) relative to a reference Earth model are imposed to lie in the intervals:

$$-1.0 < (\tau_i^{BC} - \tau_i^{DF}) - (t_i^{BC} - t_i^{DF}) < 3.0 \qquad (2)$$

$$-2.0 < (\tau_i^{AB} - \tau_i^{BC}) - (t_i^{AB} - t_i^{BC}) < 2.0 \quad (3)$$

where, t_i^{DF}, t_i^{BC} and t_i^{AB} are the travel times of the three core phases computed in the reference Earth model IASP91 *Kennett and Engdahl* [1991]. Different intervals are used because the model IASP91 slightly underpredicts PKP(DF) arrival times in this epicentral distance range *Kennett et al.* [1995]. These a priori informations are used to compute the maximum and minimum values of the parameters τ_i^{DF} and τ_i^{AB} at each step of the algorithm. The attenuation parameters t_i^* are allowed to vary between 0.0 and 2.2 s. The parameters R_{DF} and R_{AB} correct for amplitude differences between the three PKP phases, owing to source radiation, geometrical spreading and transmission coefficients. We do not introduce a priori information on these two parameters.

2.2. Optimization algorithm

The inversion is performed by minimizing the following L1 norm misfit (also called energy):

$$E = \sum_i \int |D_i(t) - S_i(t)| dt \quad (4)$$

where $D_i(t)$ and $S_i(t)$ are the observed and synthetic seismograms, and the sums are over the seismograms i and time. The waveform inversion is performed following a Simulated Annealing (SA) algorithm close to the algorithm described by Chevrot (2002). SA optimization algorithms have been widely applied in geophysics *Sen and Stoffa* [1995]; *Sharma and Kaikkonen* [1998] and more recently with teleseismic data *Kolář* [2000]; *Chevrot* [2002]. The simulated annealing algorithm is optimal for the inversion of the waveform $W(t)$ *Kuperman et al.* [1990]; *Chevrot* [2002] because energy computations are restricted to the computation of energy differences at each time step of the waveform

$W(t)$.

The algorithm used in our study is a variation of the Very Fast Simulated Annealing (VFSA) *Sen and Stoffa* [1995]. An exponential cooling schedule *Salamon and Berry* [1983]; *Nulton and Salamon* [1988]; *Andresen and Gordon* [1994] of the form $T(k) = \gamma^k T(0)$ is implemented with $\gamma = 0.98$ and N=1500 iterations. The starting temperature $T(0)$ is fixed at three times the value of the initial energy in order to start well above the critical temperature of the system, and $T(1500) \approx 10^{-14} T(0)$. At each temperature step, 5 random perturbations are implemented for each parameter P_j, and selection is done according to a Boltzmann statistics. Each perturbation consists in perturbing the waveform parameters $W(t)$ and the amplitude parameters R_{DF} and R_{AB} by $\pm\Delta W$, with $|\Delta W| = 0.01 |W|_{max}$, following the scheme described by Chevrot (2002). The other model parameters P_j are randomly perturbed at each step l according to the rule:

$$P_j^{l+1} = P_j^l + y_j (P_j^{max} - P_j^{min}) = P_j^l + y_j \Delta P_j \tag{5}$$

where the random number y_j follows a Cauchy distribution parametrized by the temperature T_j *Sen and Stoffa* [1995]:

$$y_j = sign\left(u_j - \frac{1}{2}\right) T_j \left[\left(1 + \frac{1}{T_j}\right)^{|2u_j - 1|} - 1\right] \tag{6}$$

where u_j is a real number selected randomly in the interval [0,1]. The main difference to the VFSA algorithm is that the temperature T_j is related to the energy $E(k)$ and not to the temperature $T(k)$ of the system. The temperature describing the Cauchy probability of y_j is defined by the equation:

$$T_j = \left(\frac{E(k)}{E(0)}\right)^2 \tag{7}$$

where $E(k)$ is the energy of the system. As the energy of the system decreases, the temperature T_j decreases and reduces the area explored in the parameter space. This procedure is chosen in order to adapt the random variations of the parameters to the convergence level of the system, and not to an arbitrary cooling schedule.

In order to solve cycle skipping ambiguity on noisy traces, an additional modification of the SA algorithm is introduced. Once the system has reached a good convergence level, the parameters τ_i^{DF}, τ_i^{BC} and τ_i^{AB} are reinitialized to the median value of their residuals relative to the PKP(BC) phase at all the stations, and admissible variations of the differential travel time residuals are limited to ± 1 s. This procedure introduces an additional a priori information on the time shifts, which allows to obtain coherent results even for noisy records.

The a posteriori covariance matrix is estimated following a method described by Sharma and Kaikkonen (1998). Twenty runs of the SA algorithm are performed with different random number seeds, and the covariance matrix is estimated from the results obtained for the twenty inversions. This statistical method allows to compute errors even for model parameters for which error bars are difficult to estimate, such as the t_i^* parameters. An average model is also computed, and the model presenting the lowest energy over the twenty runs is kept as the best model.

The running time of the SA algorithm depends on the number of seismograms, the time window length, and the sampling rate. For 150 seismograms, sampled at 20 Hz, with a time window of 35 s, the SA algorithm is running in 100 minutes CPU on a linux PC Pentium IV at 1.7 GHz. However, the running CPU time could be divided by a factor of five by increasing the cooling speed of the algorithm. In this case, the differential travel

times are properly resolved, but the differential attenuations are unstable.

The power of the non-linear waveform inversion with SA is illustrated in the next section with a few examples taken from the EIFEL experiment *Ritter et al.* [2000]. These examples are chosen to demonstrate the ability of the method to investigate interfering PKP branches and even their interference with depth phases.

3. Examples

To illustrate the potential of the method, we present three examples showing increasing degrees of complexity. The dataset consists of core phases recorded by the temporary EIFEL experiment in the 146°-153° epicentral distance range, and includes waveforms from about 150 broadband and short period stations installed in central Europe in the Eifel plume region *Ritter et al.* [2000]. This dense temporary network covered an area of 3° by 3° (Figure 2). The data are deconvolved from the instrument response, and filtered by a band-pass butterworth filter with corner frequencies at 0.3 Hz and 1.5 Hz. The dataset is composed of the records of eight earthquakes which occured in the Fidji-Tonga subduction zone (Table 1), three of which are presented in details in the next sections.

3.1. A simple case: the three core phases are well separated in time

152 stations of the EIFEL network have recorded the three core phases generated by the earthquake number 8 (Table 1). The data, filtered between 0.3 and 1.5 Hz, and aligned on the theoretical arrival time of the PKP(BC), are presented on Figure 3a. The three PKP phases are clearly separated in this distance range, and the noise level is low. The PKP(DF) phase is characterized by a lower frequency content and a smaller amplitude than the PKP(BC) phase owing to inner core attenuation *Souriau and Roudil* [1995];

Cormier et al. [1998]. Figure 3b shows the comparison between data and the synthetic waveforms for the best model once all the seismograms are aligned on the PKP(BC) arrival time. The fit is very good for PKP(DF) and PKP(BC) phases, and quite good for the PKP(AB) phase. The variance reduction for the whole data set is 60%, and the unexplained variance reflects the noise level. Figure 3c presents the differential time shifts $\tau_i^{DF} - \tau_i^{BC}$ and $\tau_i^{AB} - \tau_i^{BC}$. The small amount of scattering of the measurements suggests their accuracy. The measurements error bars are generally lower than 0.5 s, 0.2 s and 0.4 s respectively for PKP(DF), PKP(BC) and PKP(AB) phases.

Figure 4 presents a comparison between the rms error estimated by a statistical analysis of the 20 inversion results, and the error computed from the waveforms given by the best model using a cross-correlation method *Chevrot* [2002]. The error estimated by cross-correlation is always smaller than 0.5 s. The statistical study of the models after inversion separates the records in two groups. The records properly fitted present a low statistical error, indicating that the time shift results are stable over the 20 inversions. On the other hand, a small number of noisy records present a larger statistical error than the error estimated by cross-correlation owing to the existence of multiple local minima for the misfit function. Therefore, the statistical estimate gives an information on the misfit function and on the parameter resolution that is not accessible through the cross-correlation method.

Figure 5 presents typical evolutions of the different parameters during the cooling schedule for the 20 inversions performed. The energy shows a strong decrease close to the temperature step $k = 750$, corresponding to the critical temperature, and is approximately flat from steps 800 to 1500. At this stage, the time shifts are artificially modified in order to

overcome possible cycle skipping problems, as described before. This perturbation introduces a step like energy increase, from which the system quickly recovers. Amplitude correction parameters R_{DF} and R_{AB} are converging once the critical temperature is attained, but the final values for R_{DF} are scattered due to the correlation between R_{DF} and attenuation parameters t_i^*. In this example, $R_{DF} = 1.39 \pm 0.03$ and $R_{AB} = 0.732 \pm 0.004$, and the standard deviation of these parameters is lower than 0.06 for all the other earthquakes analysed in this study. The other plots show the evolution of the inverted parameters for a randomly chosen seismogram. These parameters present large variations before the critical temperature, beyond which they quickly converge to their final value. This value is slightly perturbed by the procedure at step $k = 750$, but convergence is achieved at the end of the algorithm. The convergence time is the longest for the t_i^* parameter, because a preliminary alignement of the PKP(DF) waveform is necessary, which simply results from the fact that energy variations due to t_i^* are small compared to the ones related to the other parameters. The set of final values for t^* generally shows the largest scatter, which indicates that it is the most poorly resolved. The different runs show that t^* converges to different values suggesting the existence of local minima for the misfit function.

3.2. Interference of the three core phases

The method has been tested in the case of interfering core phases with synthetic data computed with the WKBJ software *Chapman* [1978] including attenuation. The results are presented on figure 6. They demonstrate that the waveforms are properly fitted, and that the travel time residuals are properly recovered.

123 stations of the EIFEL network have recorded core phases generated by the earthquake number 4, see Figure 7. The records have been processed as for Figure 3. In this distance

range (146°-149°), the three PKP phases arrive within 4 to 8 seconds. Since the waveform is about 5 s long, the three core phases strongly interfere. The data fit and the time shift parameters are presented in Figures 7b and 7c respectively. The variance reduction of the whole data set is 86%. These results show that the non linear inversion is able to retreive the model parameters even when the 3 phases interfere strongly.

3.3. Complex source time functions and presence of depth phases

The method has been tested in the case of a complex source time function by including depth phases in the computation of synthetic data for an earthquake at 35 km depth. In this case, the direct PKP phases interfere with the depth phases, perturbing the waveforms and making the pick of individual phases difficult. The non linear inverse problem is solved with a reference waveform of 18 s length. The results are presented on figure 8. They demonstrate that the waveforms and differential travel times are properly recovered, and that the ouput waveforms include both direct PKP and the corresponding depth phase.

For event 6, only the 27 stations corresponding to epicentral distances smaller than 153° are selected, because the PKP(BC) phase is strongly diffracted at larger epicentral distances. The data fit and the time shift parameters are shown on Figures 9a and 9b respectively. Despite the presence of depth phases, the data fit is comparable to the previous examples (60% variance reduction), and the time shifts fit quite well those predicted by the reference Earth model. The reason is that the window length is chosen large enough to include both PKP and pPKP phases for each core phase. The inverted waveforms of the three core phases are presented on figure 9c. They exhibit two energy arrivals, the first one corresponding to the direct phase and the second one to the depth phase. The

differential time between the two phases is about 11 s. it corresponds to the hypocentral depth of 33 km when computed in the CRUST5.1 model *Mooney et al.* [1998], which is in excellent agreement with the results of the preliminary determination of epicenters. This example demonstrates that model parameters can be retreived even for long (16 s in this case) and complex source time functions allowing the measurement of the differential travel times for large magnitude earthquakes. Moreover, the algorithm is successful on a small number of records. Some tests performed on high quality data have even shown that the method works also on a single record for clearly separated phases.

4. Interpretation of the results

In the previous section, three examples of core phase data analysis have been presented in detail in order to illustrate the inversion method. The whole EIFEL core phase data, not shown here, have been analysed following the method described in section 2. We will now report the interpretation of differential travel times and attenuations in terms of Earth structure. The use of differential travel times allows to significantly reduce the errors related to event mislocations. In addition, 1 Hz PKP(DF) and PKP(BC) Fresnel zones overlap in the crust and the mantle, reducing the contribution of heterogeneous structures in these parts of the Earth. However, because the sources are close to each others, each core phase sample the same region of the Earth, and the tomographic problem is ill-posed. For this reason, we will not perform a direct inversion of these measurements to retreive the average Earth structure along these paths.

4.1. AB-BC differential travel times

The two core phases PKP(BC) and PKP(AB) follow significantly different ray paths in the Earth, with take-off angles and hit points of the rays at the CMB separated by more than 10 degrees. As a result, the AB-BC differential travel time residuals can be influenced by the Earth structure at the source or at the receiver *Helffrich and Sacks* [1994], or, owing to PKP(AB) grazing incidence at the CMB, by lower mantle heterogeneities *Bréger et al.* [2000]; *Tkalčić et al.* [2002]. Figure 10 presents differential travel times obtained for three earthquakes very close to each others in the Fidji Islands region. The differential travel time plots show similar features. The PKP(DF) phase arrives earlier than predicted by the ak135 Earth's model *Kennett et al.* [1995], and its advance increases as the epicentral distance decreases. The PKP(AB) phase presents anomalously late arrivals, that are shown in red on the plots. These positive AB-BC differential travel time residuals can be associated with anomalous structure along the PKP(AB) ray path, because such large anomalies are not seen on the BC-DF differential travel times. When plotted at PKP(AB) entry and exit points at the core-mantle boundary, the differential travel time residuals shows a clear azimutal variation. However, as seen on figure 10, the recent tomographic models of the lowermost mantle *Bijwaard et al.* [1998]; *Kárason and Van der Hilst* [2001] do not present sharp lateral velocity contrasts which are able to explain the PKP(AB) travel time anomalies. Unfortunately, it is not possible with the actual data set to determine the location, along the ray PKP(AB) paths, of the Earth structure at the origin of these travel time anomalies. Despite their poor resolution, these results show the presence of large amplitude and short wavelength heterogeneities, and

demonstrate the ability of the method to recover small scale information from the records of large seismic networks.

4.2. BC-DF differential travel times and attenuations

The two core phases PKP(BC) and PKP(DF) follow very close ray paths in the crust and the mantle, with take-off angle differences smaller than 5 degrees. These two core phases sample the same heterogeneities in the crust and the mantle, a property that has been widely used in BC-DF differential travel time residual studies *Tanaka and Hamaguchi* [1997]; *Isse and Nakanishi* [2002]. The BC-DF differential travel time residuals obtained for the whole EIFEL core phase data are presented on figure 11 as a function of epicentral distance and bottom radius of the PKP(DF) rays. A general trend is seen: the larger the BC-DF residuals the smaller the epicentral distance. The The BC-DF differential ray parameters shows large deviations from the differential ray parameter predicted by the ak135 Earth's model. The residual of BC-DF differential ray parameter ranges form -0.5 s/° at 147° epicentral distance to -0.2 s/° for epicentral distances larger than 150°. A least squares inversion of BC-DF differential travel time residuals have been performed for a simple inner core model composed of 4 homogeneous layers: one layer of 150 km thickness at the top of the inner core, and three layers of 50 km thickness below. The resulting model is plotted with error bars at the bottom of figure 11, and the data fit is shown by thick grey lines in the two plots at the top. With 65% variance reduction, the inner core model reproduces quite well the trends seen on the data. The velocity perturbation in the inner core is poorly resolved in the top 150 km because none of the PKP(DF) rays have their turning point in this layer. However, the inferred ≈0.8% velocity perturbation agrees quite well with recent studies *Niu and Wen* [2001]; *Garcia* [2002];

Isse and Nakanishi [2002]. Below 150 km depth in the inner core, a better resolution is achieved, and smaller velocity perturbations are obtained. Inner core anisotropy can not be resolved because of the poor spatial sampling of the inner core.

As seen in section 3, the t^* parameter describing the differential attenuation between PKP(BC) and PKP(DF) is the worst resolved parameter. For this reason, t_i^* parameters with statistical errors larger than 0.1 s are excluded from the analysis. Figure 12 presents the t_i^* parameters obtained for the whole EIFEL core phase data. For epicentral distance larger than about 152°, the differential attenuation decreases strongly, because the amplitude of the PKP(BC) phase is reduced by diffraction at the inner core boundary *Souriau and Poupinet* [1991]. The distribution of the inner core attenuation parameter suggests that $t^* < 1.5$ s for epicentral distances lower than 153°. The corresponding attenuations are presented through the parameter 10000/Q as a function of PKP(DF) turning point depth below the inner core boundary, following Helffrich et al. (2002). This plot puts an upper bound of ≈150 on the 10000/Q parameter, corresponding to a lower bound of ≈50 on the inner core quality factor in this region. Such an upper bound on inner core attenuation do not allow to discriminate between low attenuation models *Doornbos* [1974]; *Souriau and Romanowicz* [1996] and high attenuation models *Niazi and Johnson* [1992]; *Bhattacharyya et al.* [1993]; *Helffrich et al.* [2002] for the same region in the inner core.

5. Discussion

5.1. Advantages and limitations of the method

The method of non-linear waveform inversion and differential travel time estimates presents numerous advantages:

1. the method is simple and can be used routinely and automatically, since only the length of the reference waveform must be selected.

2. the search for a global minimum is successful even on noisy data.

3. the non-linear inversion algorithm allows to estimate waveforms and differential travel times even when the three phases interfere on the seismograms. This is also valid for shallow earthquakes for which depth phases (pPKP) are interfering with direct phases (PKP).

4. the waveform $W(t)$ can be used to estimate the source time function of the event *Kolář* [2000]. Moreover, if $W(t)$ includes both direct and depth phases (PKP+pPKP), it can be used to estimate the event depth and the structure of the crust at the source.

5. the method can be extended to the more general problem of estimating multiple teleseismic arrivals with an equation of the form $S_i(t) = W(t) * G_i(t)$, where $W(t)$ stands for a reference phase representing a crude estimate of the source time function of the event, and $G_i(t)$ is a model response describing the propagation of the different teleseismic phases present in the seismograms. In our case, using the geometrical optics framework:
$G_i(t) = A(t_i^*) * \delta(t + \tau_i^{DF}) + \delta(t + \tau_i^{BC}) + H * \delta(t + \tau_i^{AB})$.

However, some limitations come from the approximations used. A first limitation is related to the source excitation. Because the source radiation must be similar for the rays arriving at the different stations, takeoff angles must not be too close to a nodal plane. A second limitation is related to the body wave paths in the Earth: waveform distortions produced by scattering have to be small.

5.2. Conclusion

The parametrized inversion described in this study has proven to be very efficient to estimate relative arrival times and attenuations of seismic body waves, even when they interfere or when depth phases are present in the records. This method allows to analyse the PKP triplication in an epicentral distance range previously unexplored due to the complexity of the records. This approach opens new possibilities to study the fine structure of the inner core, the D" layer and the mantle discontinuities through the investigation of PKP and P triplications. Moreover, the method can be extended to more complex parametrizations, including an estimate of the source time function and focal mecanism. AB-BC differential travel time residuals indicate the presence of large amplitude and small scale heterogeneities along the PKP(AB) ray paths. The interpretation of BC-DF differential travel time residuals in terms of inner core structure leads to an inner core model with $\approx$1% velocity perturbation in the top 150 km of the inner core and small velocity perturbations below. The BC-DF differential attenuations put a lower bound of 50 on the average quality factor in the top 300 km of the inner core for this region, and for frequencies between 0.3 and 1.5 Hz.

Acknowledgments. We thank Martin Budweg and the EIFEL team for providing the core phase data, and for their technical support on this data set. This paper has been partly supported by the program "Intérieur de la Terre" of INSU (Institut National des Sciences de l'Univers).

References

Andresen, B., and J. M. Gordon, Constant thermodynamic speed for minimizing entropy production in thermodynamic processes and simulated annealing, *Phys. Rev. E*, *50*, 4346–4351, 1994.

Bhattacharyya, J., P. Shearer, and G. Masters, Inner core attenuation from short-period PKP(BC) versus PKP(DF), *Geophys. J. Int.*, *114*, 1–11, 1993.

Bijwaard, H., W. Spakman, and E. Engdahl, Closing the gap between regional and global travel time tomography, *J. Geophys. Res.*, *103*, 30,055–30,078, 1998.

Bréger, L., B. Romanowicz, and H. Tkalčić, PKP(BC-DF) travel time residuals and short scale heterogeneity in the deep Earth, *Geophys. Res. Lett.*, *26*, 3169–3172, 1999.

Bréger, L., H. Tkalčić, and B. Romanowicz, The effect of D" on PKP(AB-BC) travel time residuals and possible implications for inner core structure, *Earth Planet. Sci. Lett.*, *175*, 133–143, 2000.

Chapman, C., A new method for computing synthetic seismograms, *Geophys. J. R. astr. Soc.*, *54*, 481–518, 1978.

Chevrot, S., Optimal waveform and delay time analysis by simulated annealing, *Geophys. J. Int.*, *151*, 164–171, 2002.

Choy, G., and P. Richards, Pulse distortion and hilbert transformation in multiply reflected and refracted body waves, *Bull. Seismol. Soc. Am.*, *65*, 55–70, 1976.

Cormier, V., L. Xu, and G. Choy, Seismic attenuation of the inner core: Viscoelastic or stratigraphic?, *Geophys. Res. Lett.*, *25*, 4019–4022, 1998.

Creager, K., Anisotropy of the inner core from differential travel times of the phases PKP and PKIKP, *Nature*, *356*, 309–314, 1992.

Doornbos, D., The anelasticity of the inner core, *Geophys. J. R. astr. Soc.*, *38*, 397–415, 1974.

Doornbos, D., Observable effects of the seismic absorption band in the Earth, *Geophys. J. R. astr. Soc.*, *75*, 693–711, 1983.

Engdahl, E., R. Van der Hilst, and R. Buland, Global teleseismic earthquake relocation with improved travel times and procedures for depth determination, *Bull. Seismol. Soc. Am.*, *88*, 722–743, 1998.

Garcia, R., Constraints on upper inner core structure from waveform inversion of core phases, *Geophys. J. Int.*, *150*, 651–664, 2002.

Garcia, R., and A. Souriau, Inner core anisotropy and heterogeneity level, *Geophys. Res. Lett.*, *27*, 3121–3124, 2000.

Garcia, R., and A. Souriau, Correction to: Inner core anisotropy and heterogeneity level, *Geophys. Res. Lett.*, *28*, 85–86, 2001.

Helffrich, G., and S. Sacks, Scatter and bias in differential PKP travel times and implications for mantle and core phenomena, *Geophys. Res. Lett.*, *21*, 2167–2170, 1994.

Helffrich, G., S. Kaneshima, and J.-M. Kendall, A local, crossing path study of attenuation and anisotropy of the inner core, *Geophys. Res. Lett.*, *29*, 9.1–4, 2002.

Isse, T., and I. Nakanishi, Inner-core anisotropy beneath Australia and differential rotation, *Geophys. J. Int.*, *151*, 255–263, 2002.

Kárason, H., and R. Van der Hilst, Tomographic imaging of the lowermost mantle with differential times of refracted and diffracted core phases (PKP,Pdiff), *J. Geophys. Res.*, *106*, 6569–6587, 2001.

Kennett, B., and E. Engdahl, Traveltimes for global earthquake location and phase identification, *Geophys. J. Int.*, *105*, 429–465, 1991.

Kennett, B., E. Engdahl, and R. Buland, Constraints on seismic velocities in the Earth from traveltimes, *Geophys. J. Int.*, *122*, 108–124, 1995.

Kolář, P., Two attempts of study of seismic source from teleseismic data by simulated annealing non-linear inversion, *J. Seism.*, *4*, 197–213, 2000.

Kuperman, W., M. Collins, J. Perkins, and N. Davis, Optimal time-domain beamforming with simulated annealing including application of a priori information, *J. Acoust. Soc. Am.*, *88*, 1802–1810, 1990.

Mooney, W., G. Laske, and G. Masters, CRUST5.1: A global model at 5°x5°, *J. Geophys. Res.*, *103*, 727–747, 1998.

Niazi, M., and L. Johnson, Q in the inner core, *Phys. Earth Planet. Inter.*, *74*, 55–62, 1992.

Niu, F., and L. Wen, Hemispherical variations in seismic velocity at the top of the Earth's inner core, *Nature*, *410*, 1081–1084, 2001.

Nulton, J., and P. Salamon, Statistical mechanics of combinatorial optimization, *Phys. Rev. A*, *37*, 1351–1356, 1988.

Ritter, J., U. Achauer, U. Christensen, and Eifel Plume Team, The teleseismic tomography experiment in the Eifel region, Central Europe: Design and first results, *Seism. Res. Lett.*, *71*, 437–443, 2000.

Salamon, P., and R. Berry, Thermodynamic length and dissipated availability, *Phys. Rev. Lett.*, *51*, 1127–1130, 1983.

Sen, M., and P. Stoffa, *Global optimization methods in geophysical inversion*, Elsevier, 1995.

Sharma, S., and P. Kaikkonen, Two-dimensional non-linear inversion of VLF-R data using simulated annealing, *Geophys. J. Int.*, *133*, 649–668, 1998.

Song, X., Anisotropy of the Earth's inner core, *Rev. Geophys.*, *35*, 297–313, 1997.

Souriau, A., and G. Poupinet, The velocity profile at the base of the liquid core from PKP(BC+Cdiff) data: An argument in favour of radial inhomogeneity, *Geophys. Res. Lett.*, *18*, 2023–2026, 1991.

Souriau, A., and B. Romanowicz, Anisotropy in inner core attenuation: a new type of data to constrain the nature of the solid core, *Geophys. Res. Lett.*, *23*, 1–4, 1996.

Souriau, A., and P. Roudil, Attenuation in the uppermost inner core from broad-band GEOSCOPE PKP data, *Geophys. J. Int.*, *123*, 572–587, 1995.

Tanaka, S., and H. Hamaguchi, Degree one heterogeneity and hemispherical variation of anisotropy in the inner core from PKP(BC)-PKP(DF) times, *J. Geophys. Res.*, *102*, 2925–2938, 1997.

Tkalčić, H., B. Romanowicz, and N. Houy, Constraints on D" structure using PKP(AB-DF), PKP(BC-DF), and PcP-P traveltime data from broad-band records, *Geophys. J. Int.*, *148*, 599–616, 2002.

Van der Hilst, R., S. Widiyantoro, and E. Engdahl, Evidence for deep mantle circulation from global tomography, *Nature*, *386*, 578–584, 1997.

VanDecar, J., and R. Crosson, Determination of teleseismic relative phase arrival times using multi-channel cross-correlation and least squares, *Bull. Seismol. Soc. Am.*, *80*, 150–169, 1990.

Table 1. Characteristics of the events used in this study, extracted form the Preliminary Determination of Epicenter.

event N°	year	Month/Day	hh:mm:ss	latitude in °	longitude in °	depth in km	Mw
1	1998	01/27	02:14:13.0	-20.68	-179.27	646.0	5.3
2	1998	01/27	19:55:00.0	-22.46	178.93	608.8	5.4
3	1998	01/27	21:05:44.0	-22.34	178.90	610.0	5.5
4	1998	03/29	19:48:16.0	-17.42	-179.24	539.0	6.4
5	1998	03/29	20:38:40.0	-17.49	-179.26	526.7	5.4
6	1998	04/11	00:44:35.0	-23.60	-176.08	33.0	4.3
7	1998	04/14	03:41:21.0	-23.73	-180.00	494.4	5.3
8	1998	05/16	02:22:03.0	-22.14	-179.70	586.0	5.9

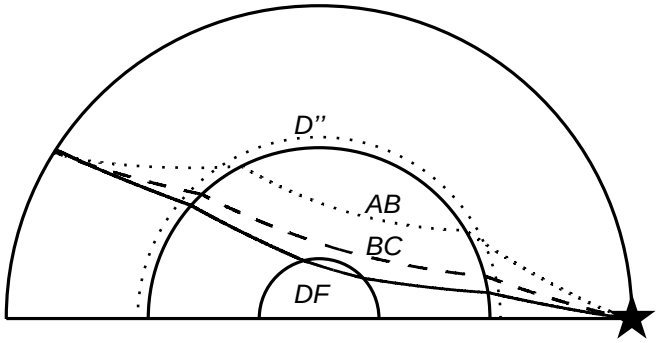

Figure 1. Ray paths of the three PKP branches in the Earth: PKP(DF) (full line), PKP(BC) (dashed line) and PKP(AB) (dotted line). The event (black star) and the D" layer at the base of the mantle are also indicated.

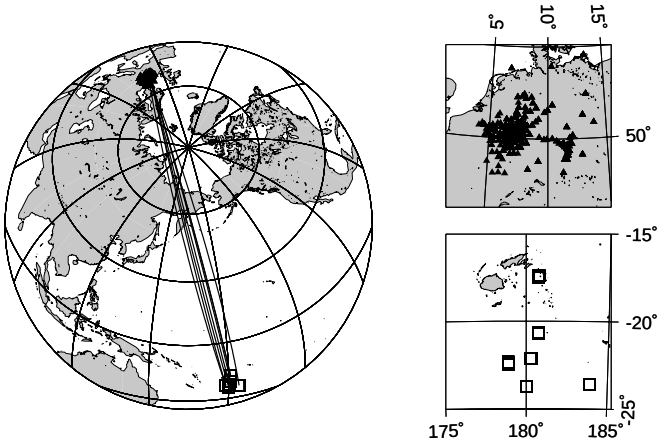

Figure 2. On the left, stations (black triangles) and events (open squares) locations with typical great circle paths (full lines). On the right, zoom of the receiver (top) and source (bottom) regions.

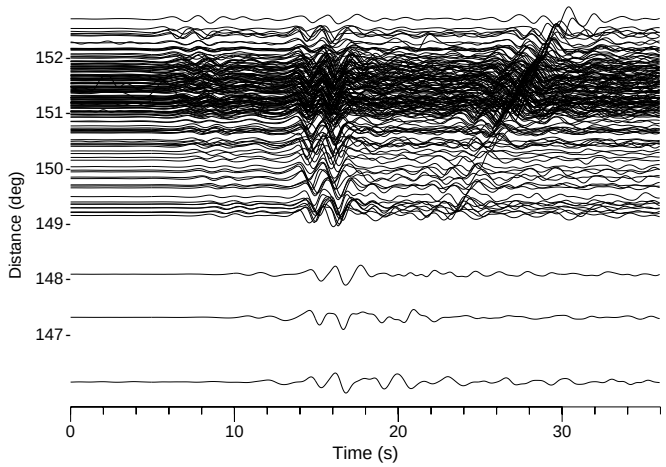

a)

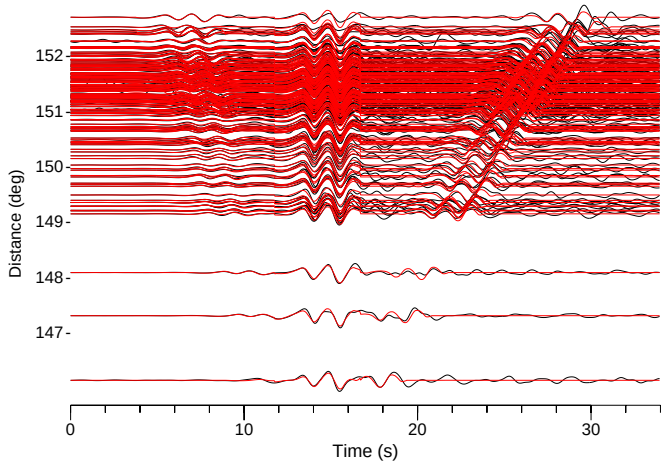

b)

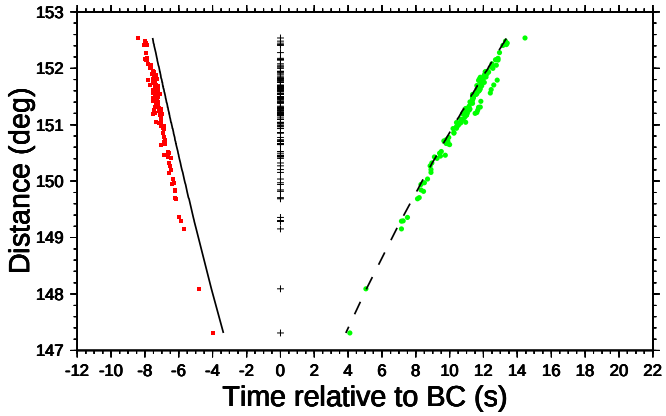

c)

Figure 3. Example 1. a) raw data before inversion, aligned on the theoretical arrival time of PKP(BC), and plotted as a function of their epicentral distance (in degrees). b) data (black lines) and best model synthetic seismograms (red lines) aligned on the PKP(BC) phase. c) best model arrival times of the three PKP phases relative to PKP(BC), dashed lines indicate theoretical arrival times predicted by the AK135 reference Earth's model.

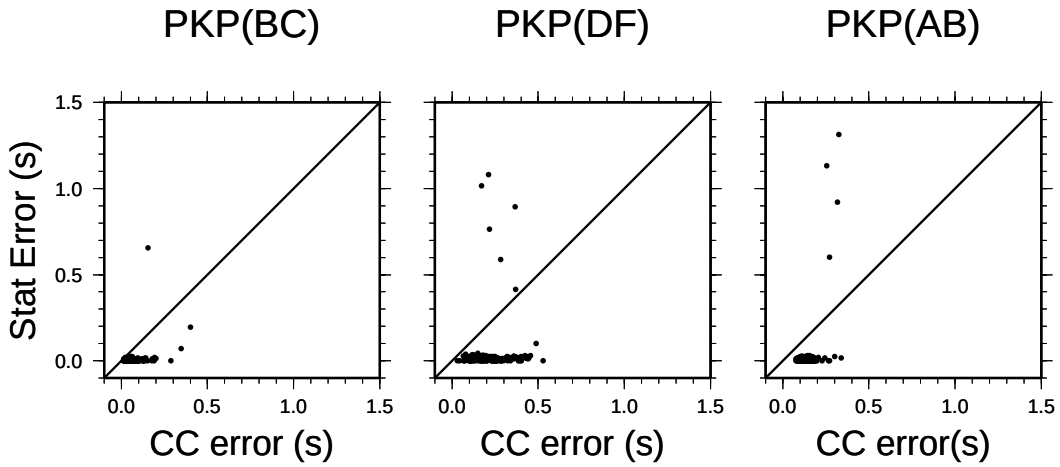

Figure 4. Statistical estimate of the time shifts rms errors (in seconds) plotted as a function of the error computed for the best model using the cross correlation method described by Chevrot (2002). From left to right, errors of the parameters τ_i^{BC}, τ_i^{DF} and τ_i^{AB}. The black line indicates the one to one correspondance.

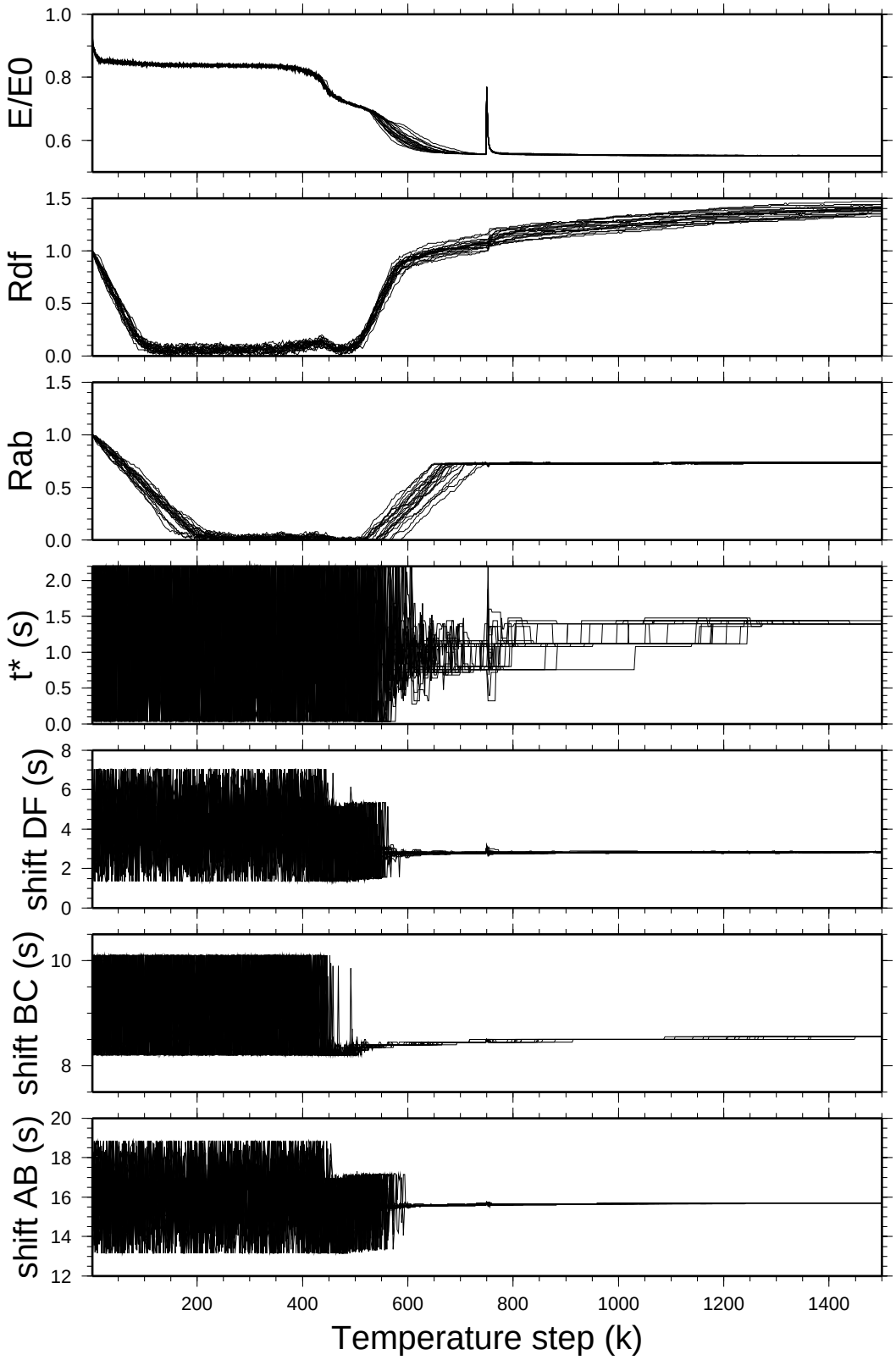

Figure 5. Energy, R_{DF}, R_{AB} and parameters of a randomly selected seismogram for the 20 SA inversions, as a function of the temperature step (k) describing the cooling schedule. From top to bottom: energy normalized to its starting value $\frac{E(k)}{E(0)}$, R_{DF}, R_{AB}, parameter t_1^* in seconds, and parameters τ_1^{DF}, τ_1^{BC} and τ_1^{AB} in seconds.

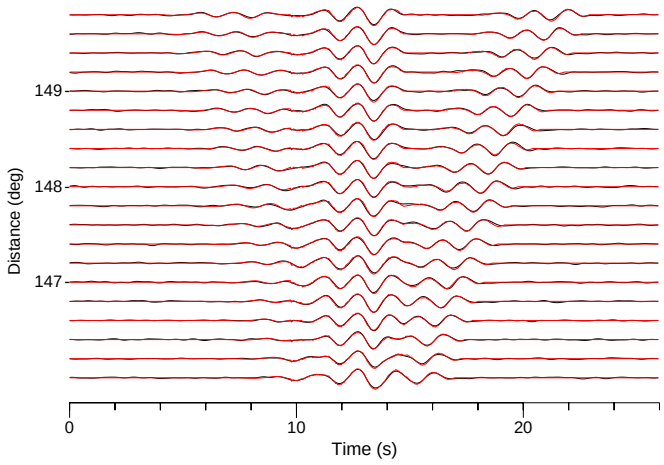

a)

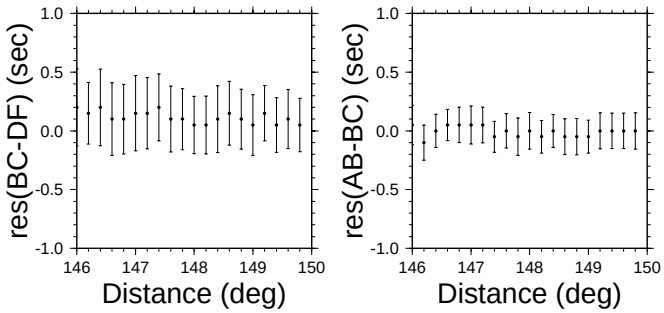

b)

Figure 6. Non linear analysis of synthetic PKP data computed with the WKBJ software for an Earthquake at 610 km depth. a) WKBJ synthetic seismograms (black lines) and synthetic seismograms predicted by the best model (red lines) aligned on the PKP(BC) phase. b) BC-DF and AB-DF best model residuals as a function of epicentral distance.

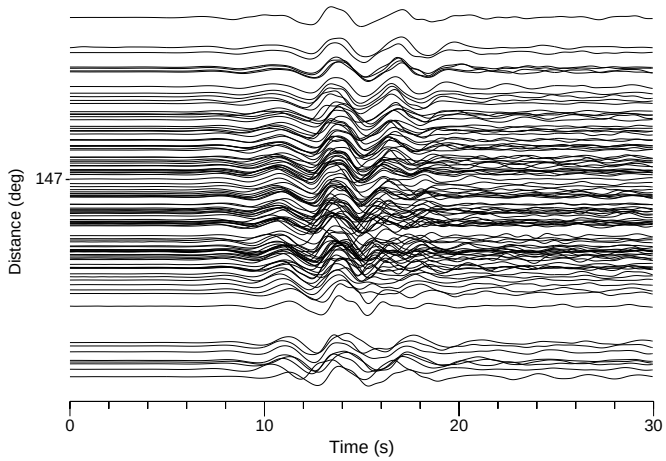

a)

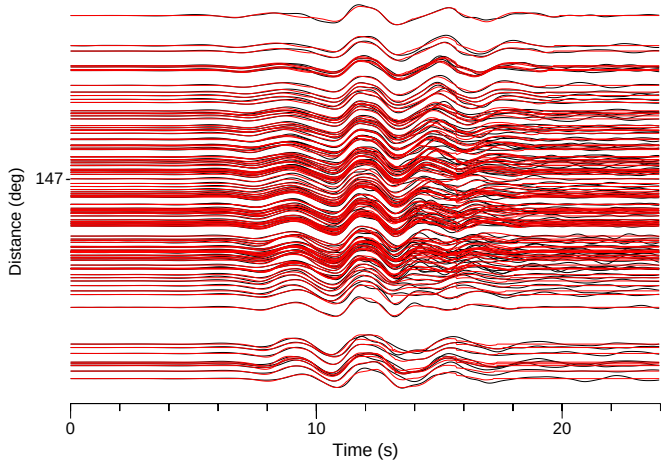

b)

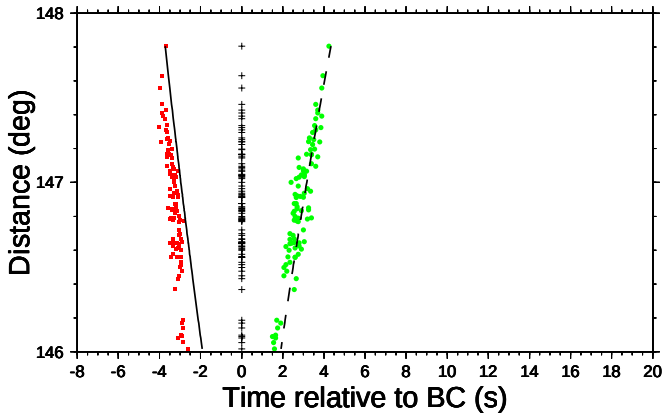

c)

Figure 7. Example 2. a) raw data before inversion, aligned on the theoretical arrival time of PKP(BC), and plotted as a function of their epicentral distance (in degrees). b) data (black lines) and best model synthetic seismograms (red lines) aligned on the PKP(BC) phase. c) best model arrival times of the three PKP phases relative to PKP(BC), dashed lines indicate theoretical arrival times predicted by the AK135 reference Earth's model.

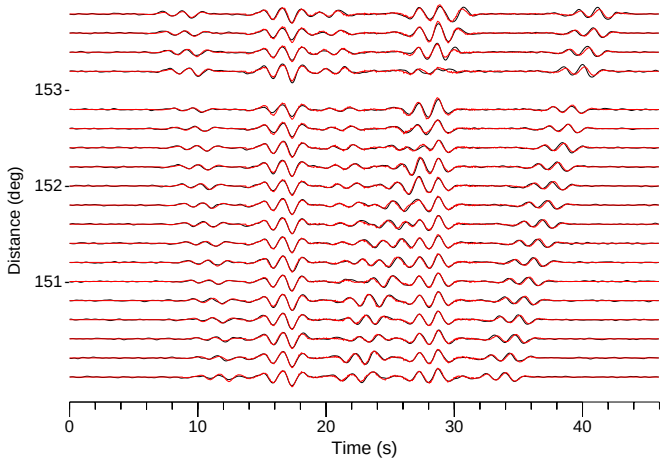

a)

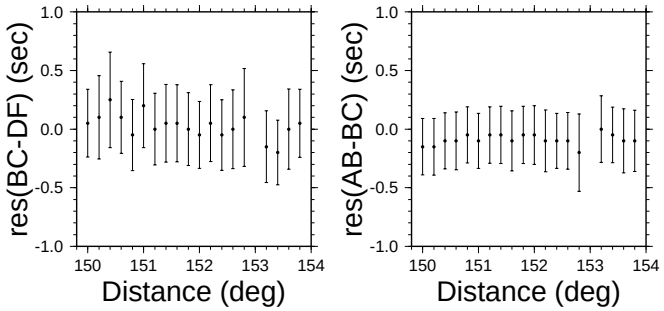

b)

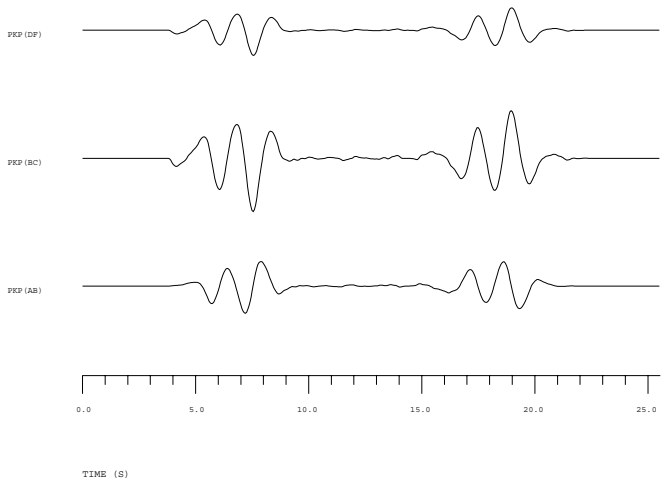

c)

Figure 8. Non linear analysis of synthetic PKP data computed with the WKBJ software for an Earthquake at 35km depth. a) WKBJ synthetic seismograms (black lines) and best model synthetic seismograms (red lines) aligned on the PKP(BC) phase. b) BC-DF and AB-DF best model residuals as a function of epicentral distance. c) From top to bottom, ouput PKP(DF), PKP(BC) and PKP(AB) waveforms including both the direct PKP phase and the corresponding pPKP depth phase.

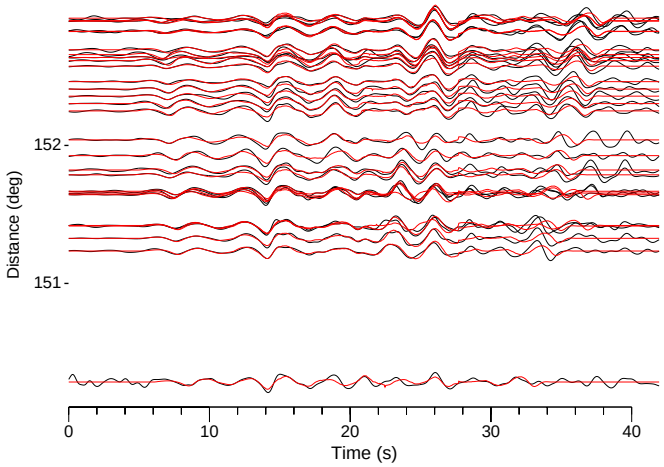

a)

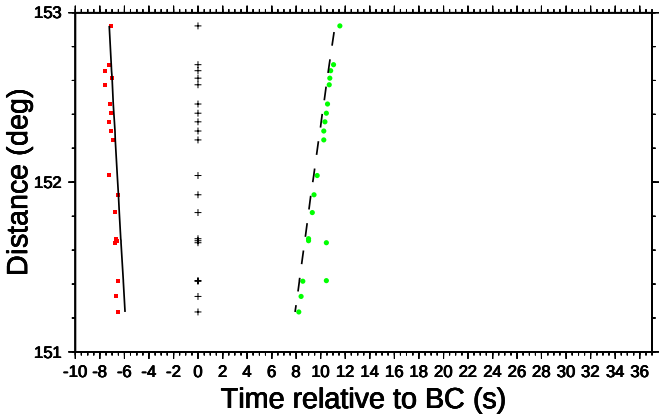

b)

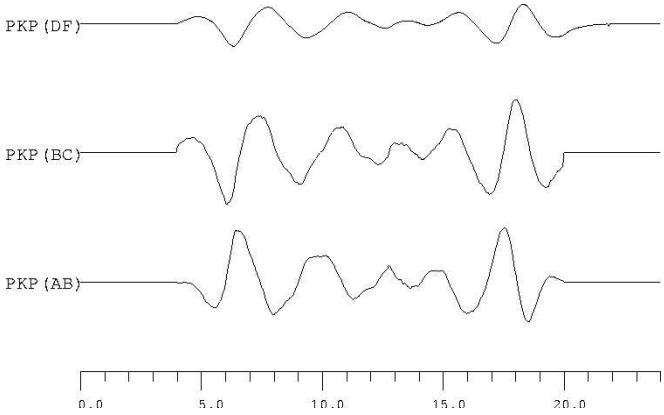

c)

Figure 9. Example 3. a) data (black lines) and best model synthetic seismograms (red lines) aligned on the PKP(BC) phase. b) best model arrival times of the three PKP phases relative to PKP(BC), dashed lines indicate theoretical arrival times predicted by the AK135 reference Earth's model). c) from top to bottom, waveforms obtained after inversions for PKP(DF), PKP(BC) and PKP(AB) phases as a fuction of time (s). Notice the two energy arrivals associated to direct and depth phases.

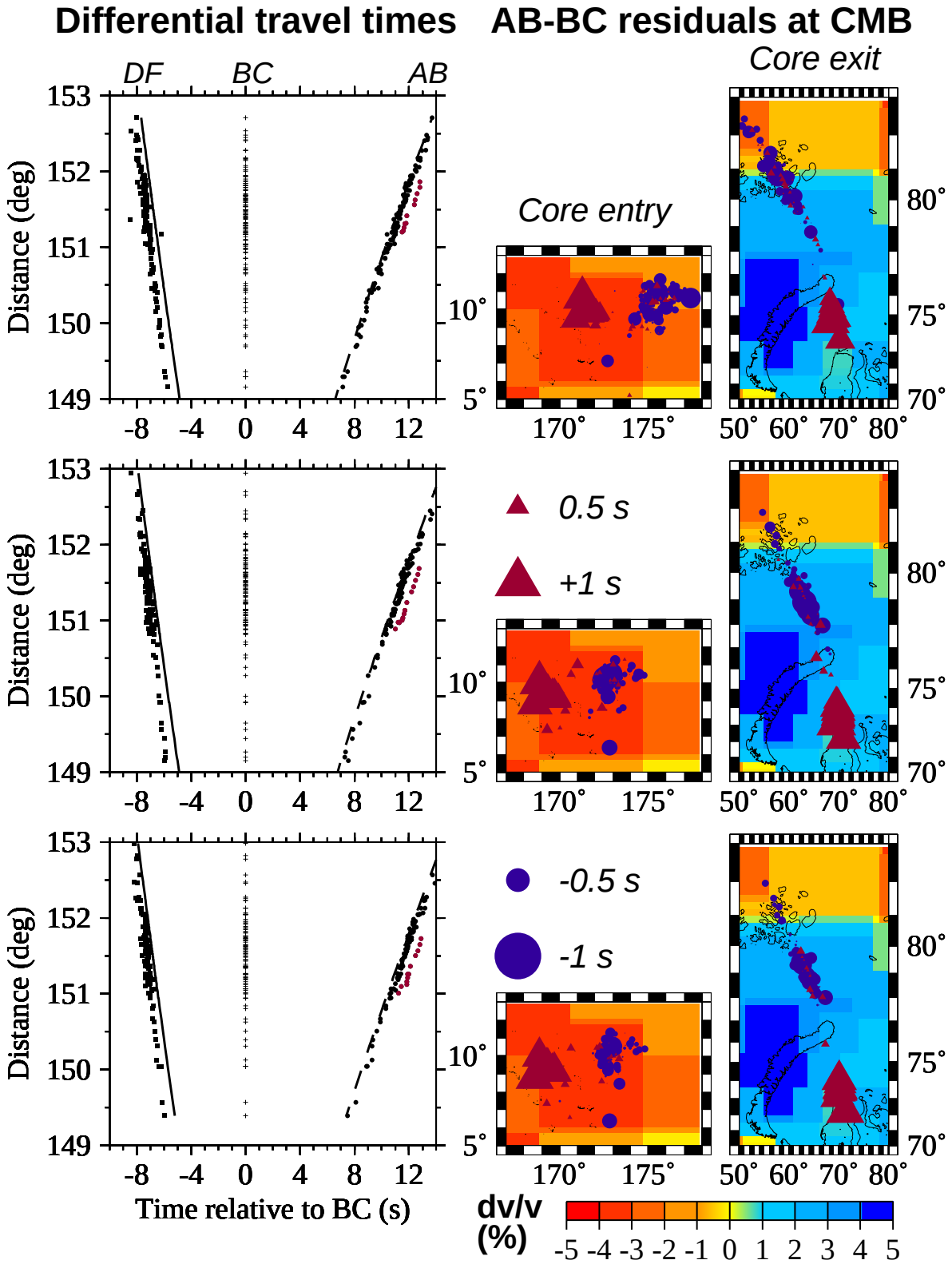

Figure 10. Interpretation of AB-BC differential travel time residuals. On the left, from top to bottom, differential travel times for events number 2, 3 and 8 on Table 1. For each earthquake, the arrival times of the three core phases relative to PKP(BC) are plotted as a function of epicentral distance. The anomalous positive AB-BC residuals are shown in red, and the theoretical arrival times predicted by the ak135 Earth model are shown as full and dashed lines. On the right, zero mean AB-BC differential travel time residuals are plotted at the entry and exit points in the core of the PKP(AB) rays, superimposed on the Bijwaard et al (1998) P-velocity model of the

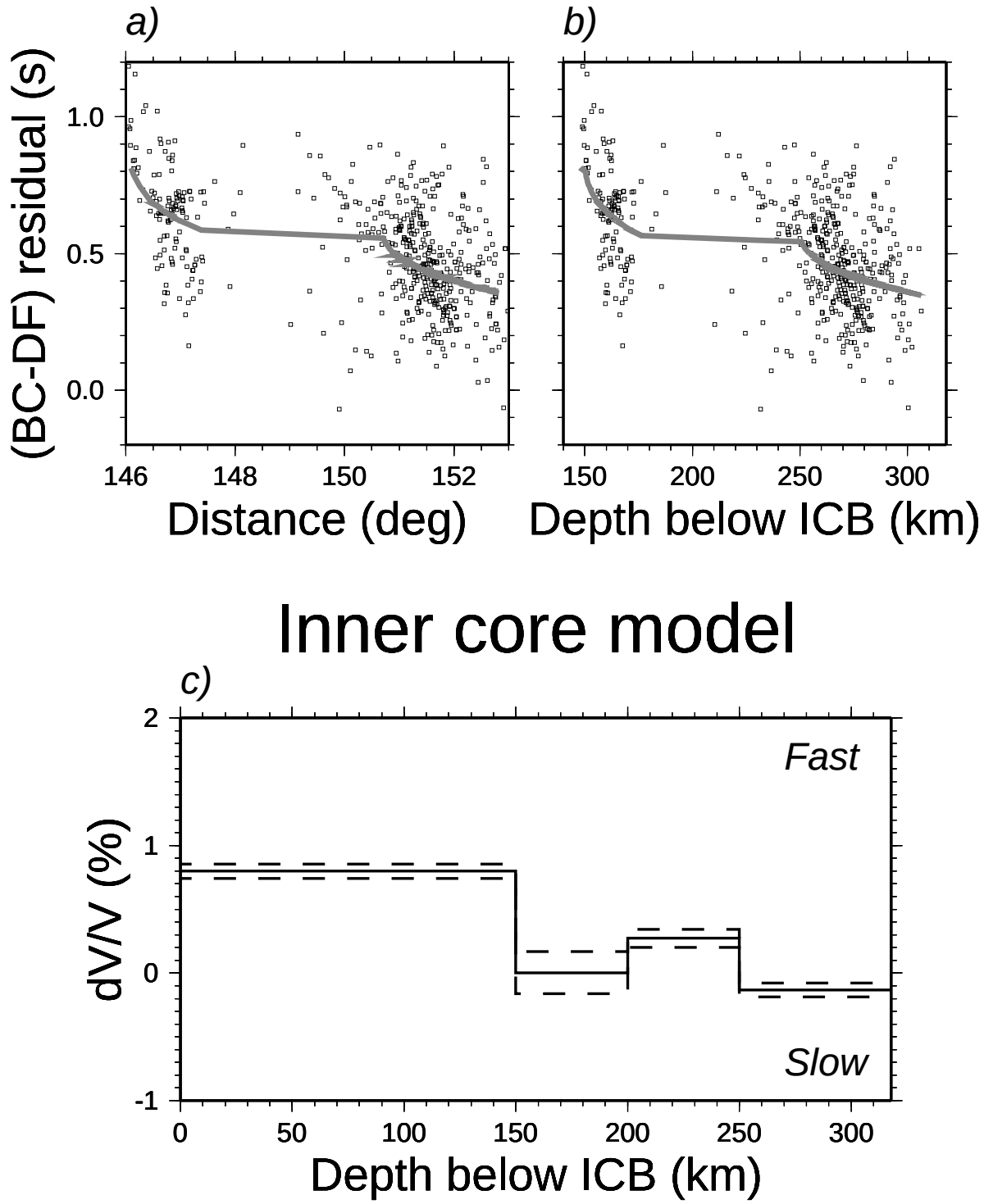

Figure 11. BC-DF differential travel time residuals for the ak135 Earth model and corresponding inner core model. At the top, BC-DF differential travel time residuals are plotted as a function of epicentral distance (a), and maximum depth of the PKP(DF) rays in the inner core (b). Thick grey lines indicate BC-DF residuals predicted by the inner core model. (c) velocity perturbation (%) as a function of depth in the inner core, obtained after inversion of the differential travel times residuals for an inner core model composed of 4 homogeneous layers. Dotted lines indicate the standard deviation of the inner core velocity perturbation.

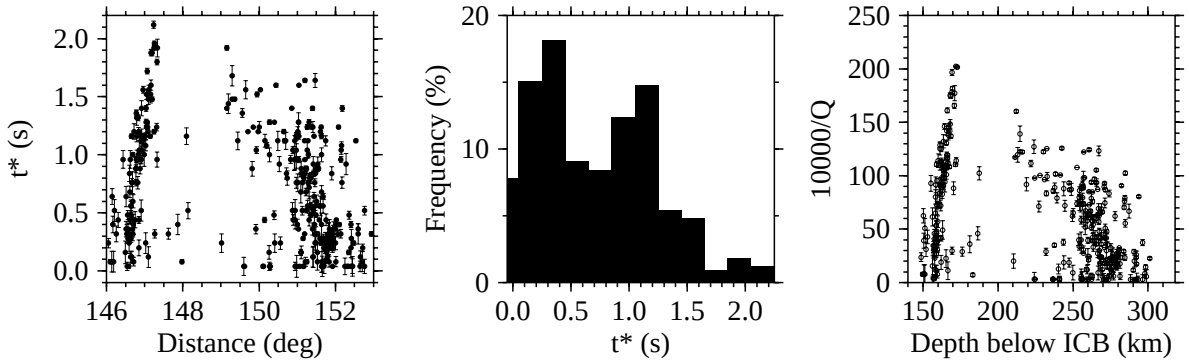

Figure 12. On the left, BC-DF differential attenuation parameters t^* (s) as a function of epicentral distance (°). In the middle, histogram of BC-DF differential attenuation parameters t^*. On the right, inner core attenuation through the parameter q=10000/Q as a function of PKP(DF) turning point depth in the inner core (km). Over the whole EIFEL core phase data set, only t^* parameters presenting statistical errors lower than 0.1 s are plotted.